Research Article | Vol. 27, No. 21 / 14 October 2019 / Optics Express 29829
Optics EXPRESS

Optical parametric chirped pulse amplifier producing ultrashort 10.5 mJ pulses at 1.55 μm

TIAGO DE FARIA PINTO,[1,2] JAN MATHIJSSEN,[1] KJELD S. E. EIKEMA,[1,2] AND STEFAN WITTE[1,2,*]

[1]*Advanced Research Center for Nanolithography, Science Park 106, 1098 XG Amsterdam, The Netherlands*
[2]*LaserLaB, Department of Physics and Astronomy, Vrije Universiteit, De Boelelaan 1081, 1081 HV Amsterdam, The Netherlands*
[*]*witte@arcnl.nl*

Abstract: We present an optical parametric chirped pulse amplifier (OPCPA) delivering 10.5 mJ pulses with durations down to 220 fs, at 100 Hz repetition rate, centered at 1550 nm. The system is pumped by a picosecond Nd:YAG amplifier at 1064 nm based on quasi-continuous-wave diode pumping and seeded by a femtosecond mode-locked Er fiber laser at 1550 nm. This choice of wavelengths enables the use of well-established technology and optical components for both pump and signal beams, resulting in a straightforward and robust system design and the ability for further power scaling to be used in high-energy laser-produced plasma experiments.

1. Introduction

The state of the art extreme ultraviolet (EUV) sources for nanolithography use high-energy lasers which are focused on liquid micro-droplets of tin inside a vacuum chamber, creating a laser-produced plasma (LPP) that emits 13.5 nm light [1]. Key plasma characteristics such as the temperature and density are heavily influenced by the input laser parameters [2–4]. These characteristics will in turn govern more practical effects such as the EUV emission spectrum and power, and the energy distribution of emitted ions. A great deal of insight on laser-plasma interaction can be obtained by studying the emission of photons and ions from LPPs for different input laser parameters [5–8].

To study such laser-plasma interactions, we built a high-energy Nd:YAG system with tunable pulse duration in the picosecond range and showed that laser parameters play a key role in the deformation of the micro-droplets [9,10] and in the energy distribution of the ions emitted by the laser-produced plasma [11,12]. We now aim to extend these studies by using femtosecond pulses to probe beyond electron-phonon interaction timescales, and study ion emission for the case where all the laser energy is deposited before ion dynamics take place. The pulse energies required for laser-plasma interaction studies are typically in the 10 mJ range and above. To generate femtosecond pulses with such high energy, we designed an optical parametric chirped-pulse amplifier (OPCPA) using the ps Nd:YAG amplifier mentioned above as the pump beam, and a commercial ultrashort fiber oscillator-amplifier system at 1.55 μm wavelength as the seed source.

Compared to 532 nm pumped OPCPA systems [13–19], direct pumping with 1064 nm offers a higher pump energy, and it yields a very useful 3.5 μm idler beam when the system is seeded at 1.55 μm. While this work focuses on the amplification of the 1.55 μm seed beam, there is a great deal of interest and work done in femtosecond sources in the mid-IR [20–22]. However, phase-matching schemes in available crystals are less optimal for ultra-broadband amplification, compared to systems pumped by frequency-doubled Nd:YAG at 532 nm and seeded by Ti:sapphire lasers. To circumvent this limitation, prior authors have used quasi-phase matching in periodically (and also aperiodically) -poled Lithium Niobate (PPLN) [20,23–25]. However, due to the limited power handling capabilities of PPLN, pulse energies are typically limited to tens of μJ. KTA- and KTP-based optical parametric amplifiers (OPAs) have been used to produce mJ-level 1.5 μm

#374587 https://doi.org/10.1364/OE.27.029829
Journal © 2019 Received 5 Aug 2019; revised 15 Sep 2019; accepted 16 Sep 2019; published 1 Oct 2019

Optics EXPRESS

and 3.5 μm pulses [21,26,27]. However, the broadest phase-matching bandwidth for 1064 nm pumping is centered at 1470 nm, where direct seed generation is challenging due to the absence of broadband laser gain media, and additional nonlinear conversion steps are required [21]. Another configuration for ultrashort pulse generation near 1.5 μm is to change the pump wavelength to the Ti:sapphire range, enabling a white-light-seeded OPA working near degeneracy [28].

When choosing the seed wavelength at 1550 nm (telecom wavelength), fs sources and efficient optics are readily available [29]. This leads to a choice between more involved seeding schemes that produce shorter pulses or a more straightforward approach based on commercial components for higher efficiency and less complexity. Because LPP applications often have more stringent demands on pulse energy and stability rather than pulse duration, in this work we explore the latter option.

2. Experimental setup

In this section, we describe in detail the pump beam generation as well as the OPCPA system. The pump laser system consists of an Nd:YVO_4 oscillator and pre-amplifier, followed by an Nd:YAG power amplifier. The amplification stages are based on two separate systems [30,31]. The OPCPA is 3-stage system using KTA crystals, where the first two stages have a non-collinear geometry, while the last stage is collinear to avoid generating a spatially dispersed idler beam.

2.1. Picosecond pump laser system

The pump laser system is seeded by a home-built Nd:YVO_4 master oscillator, operating at a wavelength of 1064 nm. The crystal is end-pumped by a fiber-coupled diode array which emits 18 W of continuous-wave (CW) radiation at 880 nm [32,33]. Mode-locking is achieved with a saturable-absorption mirror, resulting in 50 nJ, 7 ps pulses at a repetition rate of 100 MHz. To enable amplification of these pump pulses to the >100 mJ level while avoiding optical damage, a slightly longer pulse duration is preferred. Therefore a pulse duration adjustment system was implemented. In this system (Fig. 1), the beam passes through a grating in a 4-f system with an adjustable slit being placed in the Fourier plane, where the spectral content is spatially separated. By adjusting the opening of the slit, the spectrum of the laser is clipped, resulting in a tunable pulse duration up to 120 ps. For OPA pumping, the pulse duration is set to 100 ps. The downside of wavelength selection to achieve longer pulses is the lower seed power available for subsequent amplifier stages. However, this is not a limitation as the pulse energy needs to be reduced to 0.75 nJ with a waveplate and thin-film polarizer (TFP) due to power limitations of the pulse-picking system that follows next.

The spectrally-clipped 100 ps pulses are coupled to a fiber-based pulse picking scheme comprising an acousto-optical modulator (AOM) and an electro-optical modulator (EOM). The AOM (Gooch & Housego Fiber-Q) has a high contrast of 50 dB and can withstand the average power of the oscillator at the full repetition rate, but its 30 ns rise time is not sufficient to select single pulses from the 100 MHz pulse train. We therefore use it to time gate a 400 ns window, containing 40 consecutive pulses, at a 100 Hz repetition rate. The subsequent EOM (Jenoptik AM 1064) has a specified rise time of 0.25 ns with a lower contrast of 30 dB, and is controlled by an arbitrary waveform generator. The EOM can pick, from the lower average power burst after the AOM, any number of isolated pulses. In normal operation for OPA pumping, a single pulse is picked. This pulse picking assembly combines the high contrast of the AOM with the speed and flexibility of the EOM. For the present OPCPA pumping application it is mainly used to reduce the repetition rate to 100 Hz, but it can also be used for more advanced schemes, such as pulse trains with adjustable time delays (in increments of 10 ns) between each pulse [11].

After the pulse picking, the pulses are first amplified by two grazing-incidence "bounce" pre-amplifier stages. The system comprises two Nd:YVO_4 crystals, doped at 1% and 0.5%, and with dimensions of $5 \times 2 \times 20$ mm and $6 \times 4 \times 20$ mm, for the first and second crystals, respectively.

Optics EXPRESS

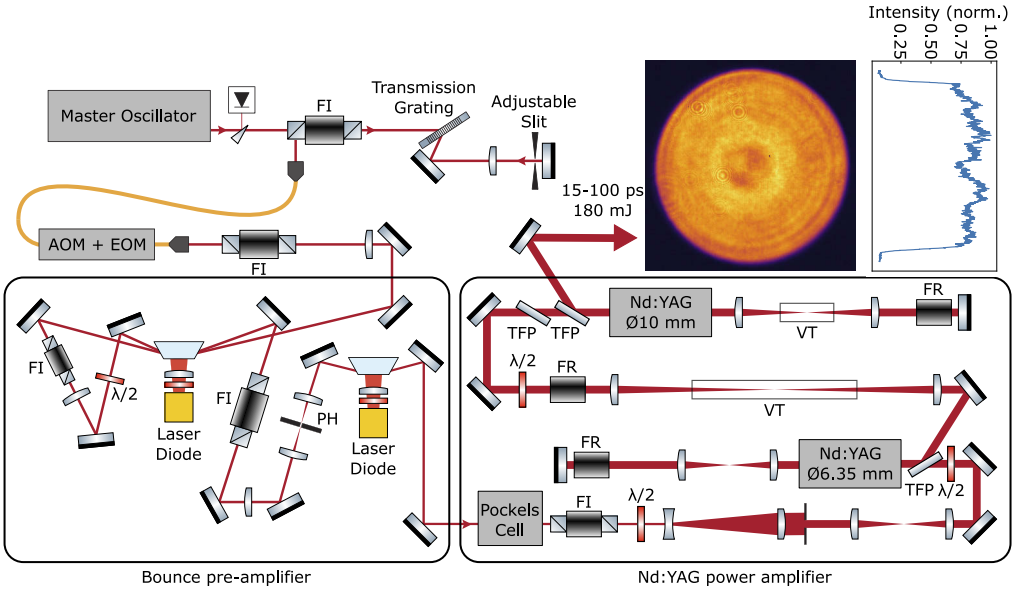

Fig. 1. Schematic of the 1064 nm pump source, consisting of the oscillator and spectral clipping system, the bounce pre-amplifier and the power amplifier units. The final output beam profile is shown on the top right, imaged from the second YAG module to a CCD camera. FR: Faraday rotator; FI: Faraday isolator; PH: 200 μm pinhole; TFP: Thin-film polarizer; VT: Vacuum tube; $\lambda/2$: Half-wave plate

The design of this bounce amplifier closely follows the concept presented by Morgenweg et al. [30]. As shown in Fig. 1, the crystals are pumped from the side by quasi-continuous-wave (QCW) pulsed laser diodes (DILAS MY-series) tuned to 880 nm through temperature control. These QCW diodes provide high pump fluence for 120 μs (slightly longer than the upper state lifetime of Nd:YVO_4) at a repetition rate of 100 Hz, resulting in a high gain with negligible thermal effects on the crystal or beam propagation. The significant doping level combined with strong single-sided pumping creates a region of very high gain confined close to the pumping surface. The beam travels through this high-gain region at an angle, and is aligned such that it undergoes a total internal reflection at the center of the pumped surface. This reflection averages away the inhomogeneity caused by the side-pumping geometry. Without this reflection, the beam would experience higher gain closer to the pumped crystal surface, leading to an uneven amplified beam profile.

The first crystal is traversed twice, using an optical isolator in between the passes to avoid parasitic lasing. After this double pass the pulse energy reaches 180 μJ. With an input energy of 120 pJ, that amounts to an average gain per pass exceeding 10^3. A consequence of the high gain is a significant amount of amplified fluorescence in addition to the amplified seed pulse. To improve pulse contrast before the second bounce amplifier stage, the amplified beam is focused through a 200 μm pinhole. Since the amplified beam and the fluorescence have slightly different a divergence and beam shape, this spatial filter can be set up such that the amplified pulse is transmitted more efficiently than the fluorescence background. After a single pass through the second crystal, we achieve a pulse energy of 1.4 mJ, which is sufficient to effectively seed a power amplifier based on large-aperture Nd:YAG rods. For optimum stability, the EOM selects a pulse from the center of the pulse train transmitted by the AOM, which results in a series of pre-pulses at 0.1% peak energy transmitted into the amplifier. In addition, after amplification we observe 0.6 mJ fluorescence in a 120 μs time window.

Optics EXPRESS

To prevent these parasitic pulses and most of the amplified fluorescence from the pre-amplifier from reaching the power-amplifier and extracting gain, two Pockels cells (PCs) and polarizers are placed between the pre- and power-amplifier stages. These PCs have rise and fall times of 5 ns, sufficiently fast to pick a single pulse, with a contrast greater than 2000:1, experimentally verified with a fast photodiode. An optical isolator is used as the last polarizer of this assembly, to protect the preceding systems against amplified back-reflections from the power-amplifier.

The power-amplifier comprises two Nd:YAG amplification modules (Northrop Grumman REA6308 and REA10008), which are both employed in a double-pass configuration [31]. These modules contain 146-mm-long cylindrical Nd:YAG rods with 6.35 and 10 mm diameter, respectively. The rods are transversely pumped by QCW diodes arranged in a five-fold symmetry. Especially in this amplifier stage, the QCW pumping enables high gain and stored energy while keeping thermal effects at a manageable level. For effective OPCPA pumping it is beneficial to have a flat-top spatial beam profile after the power amplifier. To this end, the Gaussian beam from the pre-amplifier is expanded to 12 mm ($1/e^2$-diameter) and passes through a 2 mm diameter aperture. The beam profile at the aperture plane is imaged in the center of the first Nd:YAG module. This first module has a diameter of 6.35 mm and is under-filled by a 5.4 mm beam. Although more energy can be extracted by using a larger beam inside the rod, we found that this results in the five-fold pattern of the pump geometry being imprinted on the outer edges of the beam.

To mitigate the effects of thermally-induced lensing and birefringence, a double-pass amplifier configuration is utilized [31,34,35]. The plane inside the rod at which the aperture is imaged, is subsequently relay-imaged by a telescope with unit magnification, onto a mirror which reflects the beam back for the second pass through the rod. A Faraday rotator placed close to this end mirror rotates the polarization of the beam by 90° after a double pass. This combination of spatial imaging and polarization rotation results in a compensation of the thermally-induced birefringence in the Nd:YAG rod [35]. After the double-pass, the resulting polarization is linear and rotated over 90° with respect to the incident beam, allowing convenient beam extraction with a TFP.

The image plane in the first amplifier rod is then relay-imaged in the center of the second module, using a telescope that expands the beam diameter to 8.6 mm. A Faraday rotator is placed in this telescope between the modules, which in combination with the TFPs optically isolates the passes to prevent self-lasing and damage from high-energy back-reflections. To prevent optical breakdown in air, a vacuum tube is placed at the focus of each imaging telescope after the first double-pass amplifier. Similar to the first module, the beam from the first pass through the 10 mm diameter Nd:YAG module is imaged onto a mirror and back-reflected for a second pass, with a 90° rotated polarization.

The wavelength of the pump diodes can be controlled through temperature tuning, enabling adjustment of the overlap with the Nd:YAG absorption band. Optimization the pump wavelength leads to a higher energy output, but also results in a stronger absorption with a shorter absorption length close to the outer diameter of the rods, and therefore a spatial gain profile that peaks towards the rod edges. As a result, temperature tuning of the pump diodes also enables some control over the output beam profile, and we exploit this feature to optimize the flat-top profile at the end of the amplifier chain. The resulting beam profile is depicted as an inset to Fig. 1. We operate the modules at 240 V for 235 μs at a peak current of 70 A and 85 A to reach gain saturation for the first and second modules, respectively. For optimal beam profile the temperatures are set to 21.5 °C and 20 °C, respectively. The final amplified output energy is 180 mJ, for a pulse duration of 100 ps. This energy level is intensity-limited, determined by the damage threshold of the optical coatings on the Nd:YAG rods and other components. At longer pulse durations, higher pulse energy can readily be extracted from the amplifier. The output energy can also be scaled further by utilizing amplifier rods with a larger diameter, allowing for larger beam diameters.

Optics EXPRESS

2.2. Ultrafast optical parametric chirped pulse amplifier at 1.5 μm

The OPA is seeded by a commercial Erbium-doped fiber laser (C-Fiber Sync High Power by Menlo Systems), which delivers 3 nJ, 90 fs pulses at 100 MHz repetition rate. The laser is equipped with a fast response piezo-mounted cavity mirror, which is used to synchronize its repetition frequency to that of the oscillator in the pump system. For this purpose, the repetition rates of both oscillators are monitored using fast photodiodes (EOT-3500, 12.5 GHz bandwidth). The photodiode outputs are fed into a 1.5 GHz-bandwidth frequency mixer to produce a difference frequency beat signal, which is then used as input for a PID loop which actuates on the piezo. As the difference frequency is sensitive to the relative phase between the two repetition rate signals, the relative time delay between the two laser pulse trains remains fixed each time the loop is closed. This locking scheme typically achieves timing stabilization at the 1 ps level. In addition to the piezo-mirror, the laser oscillator is also equipped with a stepper motor with a larger operating range, which enables coarse compensation of longer-term drifts and day-to-day differences in lab conditions.

The femtosecond pulses are stretched with positive group-velocity dispersion to a duration of around 30 ps in a Martinez-type 4-f grating system. The stretcher contains two equal 940 lines/mm transmission dielectric gratings with a manufacturer-specified diffraction efficiency of 95%, with an overall measured efficiency of 83%.

A schematic of the OPA layout is shown in Fig. 2. The OPA consists of three single-passed 10 mm long, $\theta = 42.5°$ KTA crystals (Castech Inc.). The first two passes are set up in a noncollinear geometry, with noncollinear angles of 2° and 1.5°, respectively. This geometry allows for the pump and idler beams from the first two passes to be easily separated from the amplified signal beam. The noncollinear geometry also has a slightly broader gain bandwidth (Fig. 3, green trace). The pump beam is *s*-polarized, while the seed beam is *p*-polarized, for all three stages.

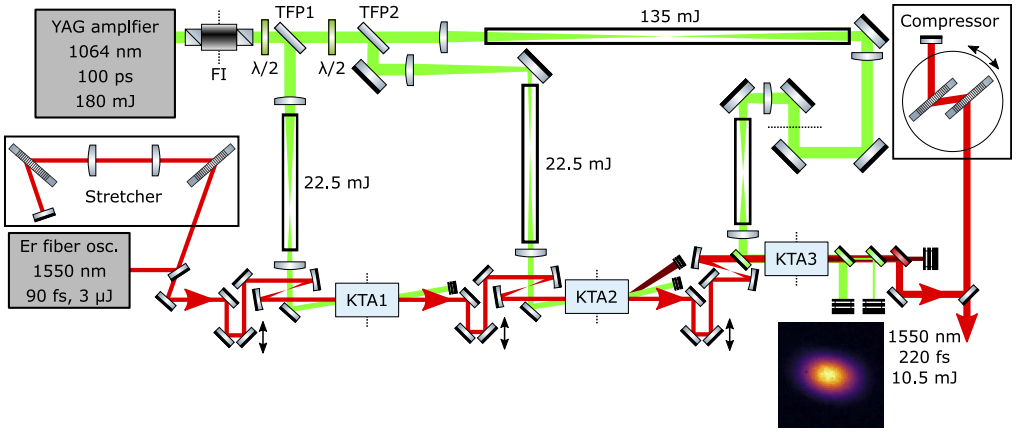

Fig. 2. A detailed schematic of the OPCPA system. The dotted lines are points where the flat-top beam profile of the pump beam is imaged. On the bottom right we show the signal output of the OPCPA, focused by a 50 mm convex lens to a 75 μm spot ($1/e^2$-diameter). The same acronyms as in Fig. 1 are used.

The pump beam is imaged on the first and second crystals, resulting in smooth flat-top spatial profiles with diameters of 1.7 mm and 1.9 mm, respectively. The seed beam has a $1/e^2$ diameter of 1.3 mm in both crystals. Both stages are pumped at 22.5 mJ and the seed is amplified to 1.4 mJ after the first two stages.

The third OPA stage is set up in a collinear geometry. While this results in a reduced gain bandwidth (Fig. 3, blue trace), it has the benefit of producing an idler beam that is not spatially

Optics EXPRESS

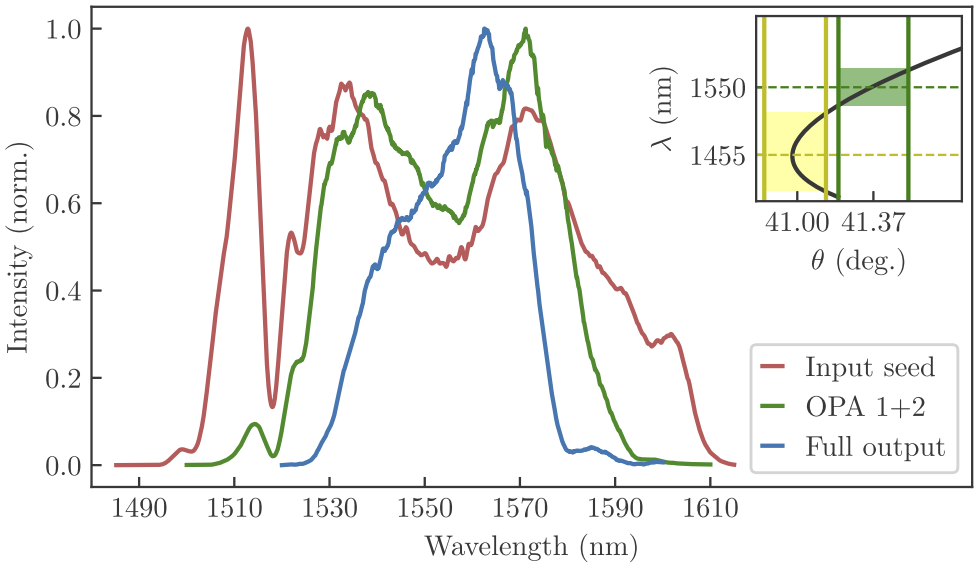

Fig. 3. Spectra at various stages in the OPCPA system. The inset shows the phase-matching curve for KTA with 1064 nm pumping. The shaded areas highlight the phase-matching bandwidths for a 0.15° acceptance angle, centered at 1455 nm (yellow) and 1550 nm (green). λ: wavelength; θ: phase-matching angle.

dispersed so that it can be used in future experiments. The pump and seed beams have diameters of 4.0 mm and 3.4 mm ($1/e^2$), respectively. The last stage is pumped by up to 135 mJ and produces up to 12.5 mJ of uncompressed 1550 nm pulses. Fluorescence at the signal wavelength was characterized by blocking the seed to the first OPA stage while pumping all stages at full power. In this configuration, the fluorescence energy remains bekow the mW-level detection limit of the power meter.

After the final crystal, there is a significant imprint of the pump spatial profile onto the signal beam, resulting in a flat-top-Gaussian mix that diffracts as it propagates. Nevertheless, the beam can be focused into a smooth Gaussian-like profile with a $1/e^2$-diameter of 75 μm by a plano-convex lens, as shown in the inset of Fig. 2.

To separate the outgoing beams, we use a set of custom-designed dielectric dichroic mirrors (Layertec). The first of these mirrors reflects the pump beam while transmitting both signal and idler, and afterwards signal and idler are separated with another dichroic mirror. In practice, two pump-separating mirrors are used to remove the pump radiation from the amplified signal beam with sufficient contrast.

The amplified signal pulses are compressed by a pair of gratings identical to those in the stretcher. Using transmission gratings enables us to use an efficient Littrow configuration in the compressor, and have a compact layout that can be conveniently mounted on a rotation stage for fine tuning the compression [14], as the input angle provides control over the ratio between second- and third-order dispersion. Like the stretcher, the compressor boasts a high efficiency of 85%, resulting in compressed pulses of 10.5 mJ. Over timescales of minutes, an energy stability of 1.5% rms was typically measured.

3. Pulse characterization

As shown in Fig. 3, after two stages, the amplified spectrum is narrower than the initial seed spectrum. This is due to the limited phase matching bandwidth. The effect is further exacerbated

Optics EXPRESS

after the third stage, due to the collinear geometry. To characterize the resulting pulse duration after the full amplifier system, we use a second-harmonic-generation frequency-resolved optical gating (SHG-FROG) device containing a 200 μm thick BBO crystal into which we send a small fraction of the amplified output beam. The measured and reconstructed SHG-FROG traces are shown in Fig. 4, along with the retrieved pulse shape. The Fourier-transform (FT) limited pulse durations corresponding to the input seed and amplified output spectra are also displayed for comparison. We find that the gain bandwidth in the collinear geometry increases the FT-limited pulse duration from 73 fs at the input of the OPA to 158 fs after all three crystals. The actual duration of the compressed pulse was measured to be 220 fs, as shown in Fig. 4. The discrepancy with the FT-limit likely comes from uncompensated residual higher-order dispersion, or possibly spectrally dependent gain saturation effects [36].

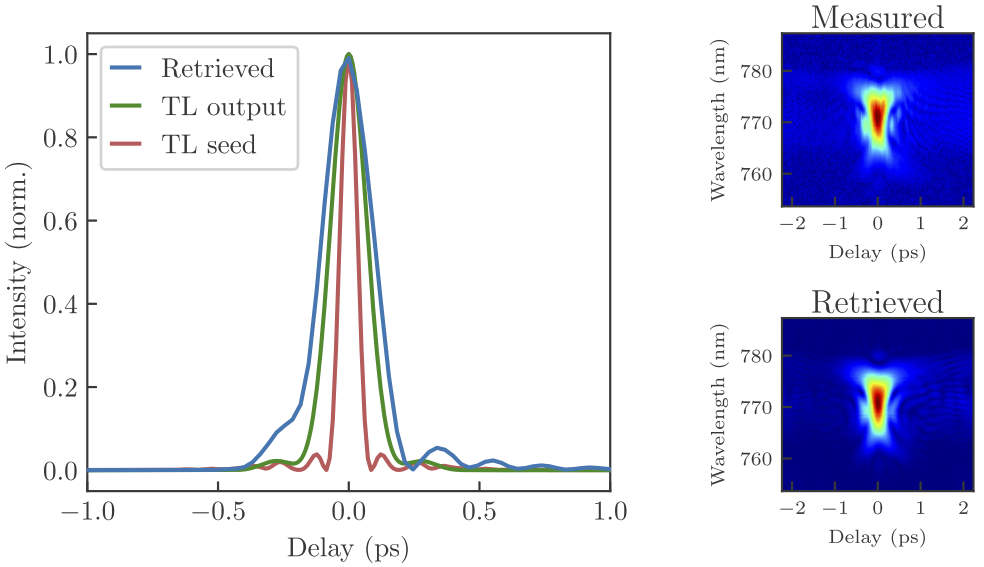

Fig. 4. Pulse characterization of the OPCPA output at full amplification, using SHG-FROG. Transform limited pulses were calculated from the spectra shown in Fig. 3.

If a spatially dispersed idler is not an issue, then with a noncollinear geometry for the third OPA stage, one could also achieve a broader bandwidth and a subsequent reduction of the achievable pulse duration.

4. Conclusion

We have described a fs OPCPA delivering 220 fs pulses with 10.5 mJ of energy at 1550 nm center wavelength, at a repetition rate of 100 Hz. The pump laser for it delivers 100 ps pulses with 180 mJ of energy at 1064 nm wavelength. In the system design, robust and direct pump and seed sources were chosen. Even though these choices limited the minimum achievable pulse duration, the achieved performance satisfies the needs for high-field and laser-driven plasma experiments at ultrafast timescales. In addition, the use of robust laser technology at these standard wavelengths enables a straightforward and reliable seeding scheme, and significant further power scaling capabilities and flexibility for plasma experiments due to the stand-alone pump source. Furthermore, the use of direct laser seeding provides a relatively high seed intensity, which is an important advantage for achieving high pulse contrast and low fluorescence background [14,15].

Optics EXPRESS

Acknowledgments

This work was conducted at the Advanced Research Center for Nanolithography, a public-private partnership between the University of Amsterdam, Vrije Universiteit Amsterdam, the Netherlands Organization for Scientific Research (NWO), and the semiconductor-equipment manufacturer ASML.

References

1. I. Fomenkov, D. Brandt, A. Ershov, A. Schafgans, Y. Tao, G. Vaschenko, S. Rokitski, M. Kats, M. Vargas, M. Purvis, R. Rafac, B. La Fontaine, S. De Dea, A. LaForge, J. Stewart, S. Chang, M. Graham, D. Riggs, T. Taylor, M. Abraham, and D. Brown, "Light sources for high-volume manufacturing EUV lithography: technology, performance, and power scaling," Adv. Opt. Technol. **6**(3-4), 173–186 (2017).
2. X. Wang, S. Zhang, X. Cheng, E. Zhu, W. Hang, and B. Huang, "Ion kinetic energy distributions in laser-induced plasma," Spectrochim. Acta, Part B **99**, 101–114 (2014).
3. E. Gamaly, "The physics of ultra-short laser interaction with solids at non-relativistic intensities," Phys. Rep. **508**(4-5), 91–243 (2011).
4. M. M. Basko, M. S. Krivokorytov, A. Yu Vinokhodov, Y. V. Sidelnikov, V. M. Krivtsun, V. V. Medvedev, D. A. Kim, V. O. Kompanets, A. A. Lash, and K. N. Koshelev, "Fragmentation dynamics of liquid–metal droplets under ultra-short laser pulses," Laser Phys. Lett. **14**(3), 036001 (2017).
5. L. Torrisi, "Ion charge state distributions in plasma produced by pulsed laser irradiations," Radiat. Eff. Defects Solids **159**(4), 249–258 (2004).
6. L. Torrisi, F. Caridi, A. Picciotto, and A. Borrielli, "Energy distribution of particles ejected by laser-generated aluminium plasma," Nucl. Instrum. Methods Phys. Res., Sect. B **252**(2), 183–189 (2006).
7. L. Torrisi, F. Caridi, D. Margarone, and A. Borrielli, "Characterization of laser-generated silicon plasma," Appl. Surf. Sci. **254**(7), 2090–2095 (2008).
8. F. Caridi, L. Torrisi, D. Margarone, A. Picciotto, A. M. Mezzasalma, and S. Gammino, "Energy distributions of particles ejected from laser-generated pulsed plasmas," Czech. J. Phys. **56**(S2), B449–B456 (2006).
9. D. Kurilovich, A. L. Klein, F. Torretti, A. Lassise, R. Hoekstra, W. Ubachs, H. Gelderblom, and O. O. Versolato, "Plasma Propulsion of a Metallic Microdroplet and its Deformation upon Laser Impact," Phys. Rev. Appl. **6**(1), 014018 (2016).
10. D. Kurilovich, T. d. F. Pinto, F. Torretti, R. Schupp, J. Scheers, A. S. Stodolna, H. Gelderblom, K. S. Eikema, S. Witte, W. Ubachs, R. Hoekstra, and O. O. Versolato, "Expansion Dynamics after Laser-Induced Cavitation in Liquid Tin Microdroplets," Phys. Rev. Appl. **10**(5), 054005 (2018).
11. A. S. Stodolna, T. de Faria Pinto, F. Ali, A. Bayerle, D. Kurilovich, J. Mathijssen, R. Hoekstra, O. O. Versolato, K. S. E. Eikema, and S. Witte, "Controlling ion kinetic energy distributions in laser produced plasma sources by means of a picosecond pulse pair," J. Appl. Phys. **124**(5), 053303 (2018).
12. A. Bayerle, M. J. Deuzeman, S. van der Heijden, D. Kurilovich, T. d. F. Pinto, A. Stodolna, S. Witte, K. S. E. Eikema, W. Ubachs, R. Hoekstra, and O. O. Versolato, "Sn ion energy distributions of ns- and ps-laser produced plasmas," Plasma Sources Sci. Technol. **27**(4), 045001 (2018).
13. S. Witte, R. T. Zinkstok, W. Hogervorst, and K. S. E. Eikema, "Generation of few-cycle terawatt light pulses using optical parametric chirped pulse amplification," Opt. Express **13**(13), 4903 (2005).
14. S. Witte, R. T. Zinkstok, A. L. Wolf, W. Hogervorst, W. Ubachs, and K. S. E. Eikema, "A source of 2 terawatt, 2.7 cycle laser pulses based on noncollinear optical parametric chirped pulse amplification," Opt. Express **14**(18), 8168–8177 (2006).
15. S. Witte, R. T. Zinkstok, W. Hogervorst, and K. S. E. Eikema, "Numerical simulations for performance optimization of a few-cycle terawatt NOPCPA system," Appl. Phys. B: Lasers Opt. **87**(4), 677–684 (2007).
16. F. Tavella, A. Marcinkevicius, and F. Krausz, "90 mJ parametric chirped pulse amplification of 10 fs pulses," Opt. Express **14**(26), 12822–12827 (2006).
17. M. Schultze, T. Binhammer, A. Steinmann, G. Palmer, M. Emons, and U. Morgner, "Few-cycle OPCPA system at 143 kHz with more than 1 μJ of pulse energy," Opt. Express **18**(3), 2836–2841 (2010).
18. S. Prinz, M. Haefner, C. Y. Teisset, R. Bessing, K. Michel, Y. Lee, X. T. Geng, S. Kim, D. E. Kim, T. Metzger, and M. Schultze, "CEP-stable, sub-6 fs, 300-kHz OPCPA system with more than 15 W of average power," Opt. Express **23**(2), 1388–1394 (2015).
19. R. Budriunas, T. Stanislauskas, J. Adamonis, A. Aleknavičius, G. Veitas, D. Gadonas, S. Balickas, A. Michailovas, and A. Varanavičius, "53 W average power CEP-stabilized OPCPA system delivering 5.5 TW few cycle pulses at 1 kHz repetition rate," Opt. Express **25**(5), 5797–5806 (2017).
20. B. W. Mayer, C. R. Phillips, L. Gallmann, M. M. Fejer, and U. Keller, "Sub-four-cycle laser pulses directly from a high-repetition-rate optical parametric chirped-pulse amplifier at 3.4 μm.," Opt. Lett. **38**(21), 4265–4268 (2013).
21. G. Andriukaitis, T. Balčiūnas, S. Ališauskas, A. Pugžlys, A. Baltuška, T. Popmintchev, M.-C. Chen, M. M. Murnane, and H. C. Kapteyn, "90 GW peak power few-cycle mid-infrared pulses from an optical parametric amplifier," Opt. Lett. **36**(15), 2755 (2011).

Optics EXPRESS

22. O. Chalus, P. K. Bates, M. Smolarski, and J. Biegert, "Mid-IR short-pulse OPCPA with micro-Joule energy at 100kHz," Opt. Express **17**(5), 3587 (2009).
23. C. Erny, C. Heese, M. Haag, L. Gallmann, and U. Keller, "High-repetition-rate optical parametric chirped-pulse amplifier producing 1-μJ, sub-100-fs pulses in the mid-infrared," Opt. Express **17**(3), 1340 (2009).
24. C. Heese, C. R. Phillips, L. Gallmann, M. M. Fejer, and U. Keller, "Ultrabroadband, highly flexible amplifier for ultrashort midinfrared laser pulses based on aperiodically poled Mg:$LiNbO_3$," Opt. Lett. **35**(14), 2340 (2010).
25. C. Heese, C. R. Phillips, B. W. Mayer, L. Gallmann, M. M. Fejer, and U. Keller, "75 MW few-cycle mid-infrared pulses from a collinear apodized APPLN-based OPCPA," Opt. Express **20**(24), 26888 (2012).
26. D. Kraemer, R. Hua, M. L. Cowan, K. Franjic, and R. J. D. Miller, "Ultrafast noncollinear optical parametric chirped pulse amplification in $KTiOAsO_4$," Opt. Lett. **31**(7), 981 (2006).
27. D. Kraemer, M. L. Cowan, R. Hua, K. Franjic, and R. J. Dwayne Miller, "High-power femtosecond infrared laser source based on noncollinear optical parametric chirped pulse amplification," J. Opt. Soc. Am. B **24**(4), 813 (2007).
28. D. Brida, G. Cirmi, C. Manzoni, S. Bonora, P. Villoresi, S. D. Silvestri, and G. Cerullo, "Sub-two-cycle light pulses at 1.6 μm from an optical parametric amplifier," Opt. Lett. **33**(7), 741–743 (2008).
29. D. Brida, G. Krauss, A. Sell, and A. Leitenstorfer, "Ultrabroadband Er:fiber lasers: Ultrabroadband Er:fiber lasers," Laser Photonics Rev. **8**(3), 409–428 (2014).
30. J. Morgenweg and K. S. E. Eikema, "A 1.8 mJ, picosecond Nd:YVO_4 bounce amplifier pump front-end system for high-accuracy XUV-frequency comb spectroscopy," Laser Phys. Lett. **9**(11), 781–785 (2012).
31. D. W. E. Noom, S. Witte, J. Morgenweg, R. K. Altmann, and K. S. E. Eikema, "High-energy, high-repetition-rate picosecond pulses from a quasi-CW diode-pumped Nd:YAG system," Opt. Lett. **38**(16), 3021 (2013).
32. L. Sun, L. Zhang, H. J. Yu, L. Guo, J. L. Ma, J. Zhang, W. Hou, X. C. Lin, and J. M. Li, "880 nm LD pumped passive mode-locked TEM00 Nd:YVO_4 laser based on SESAM," Laser Phys. Lett. **7**(10), 711–714 (2010).
33. J. Morgenweg, *Ramsey-comb spectroscopy* (PhD Thesis, Vrije Universiteit Amsterdam, 2014).
34. Q. Lü, N. Kugler, H. Weber, S. Dong, N. Müller, and U. Wittrock, "A novel approach for compensation of birefringence in cylindrical Nd:YAG rods," Opt. Quantum Electron. **28**(1), 57–69 (1996).
35. J. Sherman, "Thermal compensation of a cw-pumped Nd:YAG laser," Appl. Opt. **37**(33), 7789 (1998).
36. S. Witte and K. S. E. Eikema, "Ultrafast Optical Parametric Chirped-Pulse Amplification," IEEE J. Sel. Top. Quantum Electron. **18**(1), 296–307 (2012).